MULTI-SCALE MORPHOLOGICAL ANALYSIS FOR RETINAL VESSEL DETECTION IN WIDE-FIELD FLUORESCEIN ANGIOGRAPHY

Li Ding[1]*, Ajay Kuriyan*[2]*, Rajeev Ramchandran*[2]*, and Gaurav Sharma*[1]

[1]Dept. of Electrical and Computer Engineering, [2]Dept. of Ophthalmology,
University of Rochester, Rochester, NY

ABSTRACT

We describe a new method for accurate retinal vessel detection in wide-field fluorescein angiography (FA), which is a challenging problem because of the variations in vasculature between different orientations and large and small vessels, and the changes in the vasculature appearance as the injection of the dye perfuses the retina. Decomposing the original FA image into multiple resolutions, the vessels at each scale are segmented independently by first correcting for inhomogeneous illumination, then applying morphological operations to extract rectilinear structure and finally applying adaptive binarization. Specifically, a modified top-hat filter is applied using linear structuring elements with 9 directions. The maximum value of the resulting response images at each pixel location is then used for adaptive binarization. Final vessel segments are identified by fusing vessel segments at each scale. Quantitative results on VAMPIRE dataset, which includes high resolution wide-field FA images and hand-labeled ground truth vessel segments, demonstrate that the proposed method provides a significant improvement on vessel detection (approximately 10% higher recall, with same precision) than the method originally published with VAMPIRE dataset.

Index Terms— Blood vessel detection, wide-field fluorescein angiography, opthalmological image analysis

1. INTRODUCTION

Common systemic diseases, such as diabetes, hypertension, and artherosclerosis affect blood vessels throughout the body [1]. Retinal vein occlusion (RVO) and diabetic retinopathy are two common retinal conditions that are characterized by retinal vasculature tortuosity, ischemia, intraretinal hemorrhages, cotton wool spots, and cystoid macular edema (CME) [2]. Both diseases can also result in the loss of retinal vasculature.

Wide-field fluorescein angiography (FA) provides a useful imaging modality for visualizing and assessing the impact of these systemic diseases on the vascular system. A fluorescein dye is injected intravenously and images are captured as the dye perfuses through the retinal blood vessels [3]. Figure 1 shows two samples FA images[1]. Compared to alternatives such as color fundus images, FA images have the advantage that they provide a wide field of view (FOV). Typically, color fundus images capture only a 30° to 60° FOV, whereas wide-field FA provides permits up to 200° FOV. The wide FOV allows visualization of the entire retinal vasculature in a single image. As shown in Fig. 1 (b), peripheral vessels are also captured with sufficient details. The wide FOV allows imaging of the peripheral region of retina, which makes it possible to measure the relative changes in peripheral retinal vessels.

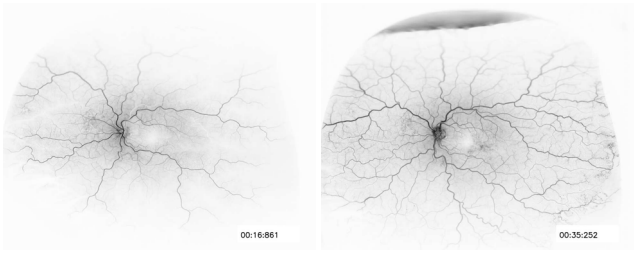

(a) (b)

Fig. 1. Sample wide-field fluorescein angiography (FA) images. The images are captured at different time elapsed from the dye injection, as indicated by the time stamp in the bottom right corner.

In current clinical practice, ophthalmologists manually examine retinal images to assess abnormalities and changes in blood vessels occurring over time. Such assessments are typically qualitative and their sensitivity is therefore limited by the available time. Quantitative manual assessments are extremely time-consuming and impractical in the clinical setting. Automated methods for detection of blood vessels are highly desirable for providing quantitative assessments that correlate with disease/treatment progression and assist physicians in diagnosis and treatment. Vessel detection is an essential step in automatic retinal image analysis which makes accurate and reliable measurements of vasculature changes possible.

In this paper, we propose a new method for accurate retinal vessel detection in wide-field FA image, which is a challenging problem mainly because the vasculature appearances vary between lager and small vessels. The proposed method uses multi-scale, multi-orientation morphological analysis to account for different widths and directions of vessel structures. The image is processed at different scales independently and the final vessel segmentation is obtained by fusing together the results from different scales. The vessels are detected by first correcting for uneven illumination, then applying morphological top-hat operations and finally applying adaptive thresholding. Morphological top-hat operations with linear structuring elements with different orientations are able to extract bright and rectilinear structures in the image that represent the blood vessels.

The paper is organized as follows. Section 2 summarizes the previous work on vessel detection in retinal images. Section 3 summarizes the proposed method. We present experimental results on VAMPIRE dataset [4] in Section 4, and conclude the paper in Section 5.

[1]The grayscale from black to white is inverted in images presented in the paper (except Fig. 3) to provide a better visualization in common display and print environments.

978-1-5386-6490-2/17/$31.00 ©2017 IEEE

2. RELATED WORK

The problem of detecting vessels from retinal images has been studied extensively and a number of methods have been proposed. The predominant majority of proposed techniques focus on fundus images rather than wide-field FA. In this section, we review the major existing approaches which generally fall into two main categories: supervised and unsupervised [5].

Supervised methods rely on a set of labeled ground truth images that are manually annotated by experts. In [6], a pixel classification method is proposed that uses a Gaussian filter and K-nearest neighbor classifier. A probability map is estimated which indicates the probability of each pixel being vessel or non-vessel. In [7], a method based on fully connected conditional random (CRF) field is used. The parameters of fully connected CRF model is trained by a structured output support vector machine. Recent work in [8, 9, 10, 11] has exploited deep learning approaches for this problem. Methods in [8, 9] trained deep neural network to determine the class (vessel or non-vessel) of each pixel based on its neighborhood. In [10], the problem of vessel detection is formulated as an image-to-image regression task. A convolution neural network (CNN), which is built on the top of VGG [12], is proposed to detect retinal vessels and optic disc. In [11], a generative adversarial network [13] framework is proposed. The usage of a discriminator network is able to improve the accuracy of vessel segmentation.

Unsupervised methods, on the other hand, do not require any manual annotation as ground truth. For instance, matched filtering was first proposed by [14] and further developed by [15, 16, 17, 4]. In [18], a method aiming at detecting small vessels is proposed based on basic filtering schemes. Morphological operations are also commonly used in vessel detection [19, 20]. The basic idea is to apply morphological operators to extract linear and connected region that is proper representation of vessels in the image. For detailed survey of retinal vessel detection methods, please refer to [5].

As already noted, most of algorithms concentrate on vessel detection in fundus images rather than wide-field FA images. Because to the different data modalities, the methods that focus on fundus images do not have comparable performance on wide-field FA images. This motivates our work on vessel detection in wide-field FA images.

3. PROPOSED METHOD

Over the retinal vasculature, blood vessels naturally exhibit variation in orientation and changes in scale between the major and minor branches. To detect the vessels, we use the algorithmic pipeline shown in Fig. 2 *which relies on multiple scales and orientations morphological analysis that is particularly attuned to the aforementioned characteristics of the retinal vessels*. The original FA image is first decomposed into several resolutions to detect both major and minor vessels of different widths. The vessels at each scale are detected, independently, by correcting uneven illumination, applying modified morphological top-hat operations and finally adaptive thresholding. Each modified top-hat operator detects bright and rectilinear structures that represent the blood vessels in the image with matching orientation. The final version of vessel segments is obtained by combining the results of vessel image at each scale.

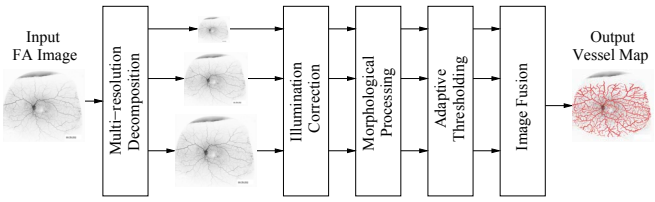

Fig. 2. Overview of the proposed method for detecting vessels in FA image. The detected vessels shown in red are superimposed on the image.

3.1. Multiple Resolution Decomposition and Fusion

One of major challenges in detecting vessels from FA images is the vasculature appearance variations. In order to robustly and accurately detect both major and minor vessels from the images captured at different time elapsed from the dye injection, we apply a mutliscale framework by decomposing the original FA image, denoted as $I_0\,(x, y)$, into multiple resolutions. Specifically we adopt image pyramid [21] that represents image as a set of reduced resolution images. The image at scale s, denoted as I_s, is obtained by convolving image I_{s-1} with a 5×5 Gaussian-like kernel G followed by subsampling by a factor of 2:

$$I_s = \mathbf{P}\,(I_{s-1} * G)\,, \tag{1}$$

where the symbol $*$ denotes the convolution and $\mathbf{P}$ is a subsampling operator.

We observe that occlusions may occur in peripheral region of retina due to eyelids and eyelashes being captured in the FA image. To overcome this issue, we create a mask to crop the image from central region of interest (ROI). The binary mask is computed by fitting an ellipse shape to the largest connected region of non-zeros pixel values.

For each image I_s, along with the associated mask, are processed independently to detect vessel segments (described in the following Sections 3.2 through 3.4). The resulting binary vessel segmentation at different scales are fused together to achieve the final vessel segmentation. To do so, Gaussian pyramid expansion is used to resize vessel image from each scale s to the size of original image I_0. Pixels where vessel are detected at any scale (foreground) are assigned as final detected vessels.

3.2. Uneven Illumination Correction

Non-uniform illumination is a common issue in FA images that results in imbalanced spatial distribution of local intensity. For example, high brightness and contrast is commonly seen in the vicinity of the optic disc whereas vessels in peripheral regions normally have low intensity and are blurred. The inhomogeneous illumination brings difficulties to detect vessels in all regions in the image and affects the performance of vessel detection methods.

Additionally, during image acquisition, as the injected dye propagates in the retina, the intensity of vessels changes among frames captured at different time elapsed from the dye injection. At the early phase, only a small portions of vasculature where the dye has been perfused can be seen. The contrast between vessels intensity and background intensity is relatively low, making the vessel detection more challenging. Before extracting vessel segments, it is essential

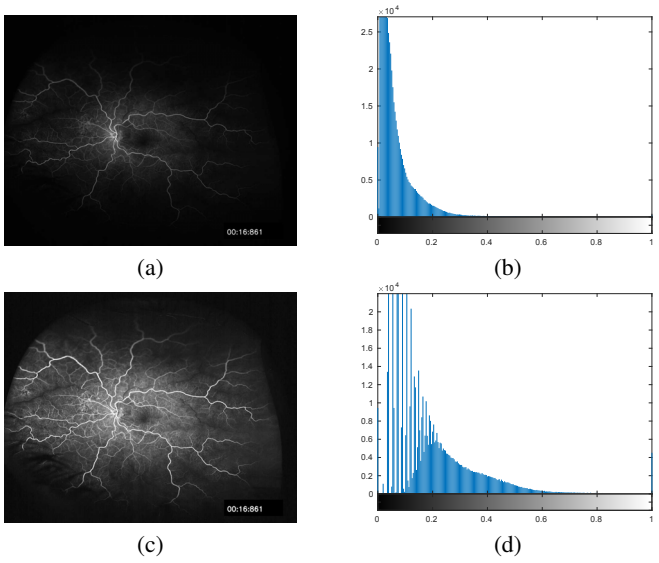

Fig. 3. Images before (top) and after (bottom) uneven illumniation correction. The images are shown without inverting grayscale. (b) and (d) shows the corresponding histograms of image.

to produce a uniform background illumination and to enhance vessel structures.

To correct uneven illumination, we employ an illumination equalization method [22]. The local average intensity of the image I_{av} is first estimated by applying a $N \times N$ window mean filter to the image. The adjusted image is then computed by

$$I_{eq}(x,y) = \frac{I_s(x,y)}{I_{av}(x,y) + c}, \tag{2}$$

where c is a constant. The uneven illumination correction increases the intensity in dark region and returns an uniform background. Figure 3 shows the images with histograms before and after illumination correction.

3.3. Morphological Processing

In the proposed method, morphological operators extract structures that represent the shape of vessels in the image. We choose a set of linear structuring elements because vessels have rectilinear structure and are connected in the retina. Specifically, we generate a set of M linear structuring elements S_θ with the same length L but different angles θ, ranging from 0° to 180°.

We perform top-hat operator on the image using structuring elements S_θ. The traditional top-hat operator [23, pp. 557], which is defined as the difference between original image and the corresponding morphological opening image, is sensitive to noise. In order to enhance the vessel detection, a modified top-hat filtering [24] is chosen:

$$I_{eq} \odot S_\theta = I_{eq} - \min\left((I_{eq} \bullet S_\theta) \circ S_\theta, I_{eq}\right), \tag{3}$$

where the symbols $\odot$ is the modified top-hat operator, and $\bullet$ and $\circ$ indicate the morphological operators of image closing and opening, respectively.

We use M structuring elements for modified top-hat operator which results in M different response. Figure 4 shows sample responses from two structuring elements. Fig. 4 (a) and (b) correspond to the responses from a vertical and a horizontal structuring elements, respectively. The maximum value of M responses at each pixel location is assigned to the final response.

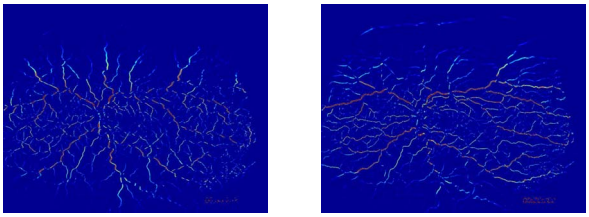

Fig. 4. Sample response images from modified top-hat operation using two structuring elements with different orientations. Red and yellow regions indicate strong responses.

3.4. Adaptive Thresholding

The morphological processing yields image where pixel intensity indicates the responses from the modified top-hat operation. Pixels with high values are likely to be vessels. In the final step, we convert this response image into the binary vasculature map.

A global binarization such as Otsu's method [25] is not suitable for this problem because it tends to miss small vessels with low intensity in the FA image. This can be seen in Fig. 4 where the responses of fine vessels are relatively low. Therefore, we take into account local pixel intensity information and adopt the adaptive thresholding method that relies on local average intensity.

The binary vessel image obtained normally has many disconnected segments. As a post-processing step, we perform an area opening operation to remove small segments that have fewer than 200 pixels from final vessel image.

4. EXPERIMENTAL VALIDATION

4.1. Experimental Setup

The proposed method is tested on VAMPIRE dataset [4], which contains 8 wide-field FA images with resolution of 3900×3072, capturing a 200° FOV of the retina. There are two sequences in this dataset representing a healthy retina (GER) and a retina with age-related macular degeneration (AMD[2]). Each sequence is a time course of exposures captured progressively as the FA dye perfused into the vessels. Each image is associated with a ground truth binary image of vessel segmentation annotated by ophthalmologists.

To quantitatively evaluate the performance of the proposed method, we compare the results of vessel detection with the ground truth image. We compute 6 metrics for each test image: *Pr* (Precision), *Rc* (Recall), *Sp* (Specificity), *Ac* (Accuracy), *DC* (Dice Coefficient) and *G* (G-mean). Precision is the ratio of the number of pixels in correctly detected vessels to the number of pixels of all detected vessels. Recall is defined as the number of pixels of correctly detected vessels divided by the number of vessel pixels in ground truth. Specification is defined as the fraction of the number of correctly classified non-vessels pixels out of the total number of non-vessels pixels. Accuracy is the fraction of all correctly classified pixels including vessels and non-vessels. Apart from these

[2] Although AMD does not cause peripheral retinal vasculature changes, this is the only publically available manually annotated wide field FA dataset for which we can compare the proposed algorithm against previously published results

	Perez-Rovira [4]						Proposed					
Frame	*Pr*	*Rc*	*Sp*	*Ac*	*Dc*	*G*	*Pr*	*Rc*	*Sp*	*Ac*	*Dc*	*G*
AMD1	0.425	**0.694**	0.992	0.994	0.527	**0.831**	**0.729**	0.472	**0.999**	**0.996**	**0.573**	0.687
AMD2	0.601	0.750	0.981	**0.987**	0.667	0.860	**0.669**	**0.784**	**0.990**	0.985	**0.722**	**0.881**
AMD3	**0.712**	0.668	0.972	**0.987**	0.689	0.812	0.685	**0.777**	**0.983**	0.973	**0.728**	**0.874**
AMD4	0.589	0.381	0.969	**0.990**	0.462	0.614	**0.766**	**0.404**	**0.996**	0.975	**0.529**	**0.634**
GER1	0.577	**0.643**	0.993	**0.996**	**0.608**	**0.800**	**0.784**	0.461	**0.999**	0.994	0.580	0.678
GER2	**0.745**	0.547	0.972	**0.992**	0.631	0.736	0.676	**0.662**	**0.986**	0.972	**0.669**	**0.808**
GER3	**0.693**	0.477	0.954	**0.986**	0.565	0.686	0.641	**0.696**	**0.974**	0.957	**0.667**	**0.823**
GER4	**0.716**	0.511	0.977	**0.993**	0.597	0.713	0.666	**0.719**	**0.988**	0.979	**0.691**	**0.843**
Average	0.665	0.551	0.976	**0.991**	0.603	0.739	**0.676**	**0.664**	**0.989**	0.979	**0.670**	**0.810**

Table 1. Quantitative comparison of the results obtained from [4] and the proposed method on VAMPIRE dataset. The best result is shown in bold.

four metrics, we also use two additional measures: dice coefficient and G-mean that are more suitable to evaluate the performance on imbalanced data [7]. Dice coefficient and G-mean are the harmonic mean of precision and recall and the geometric mean of specificity and recall, respectively. Both metrics range from 0 to 1, with 0 indicating no agreement between predicted results and ground truth, and 1 a perfect results with no error. These metrics can be computed from the true positive (TP), false positive (FP), true negative (TN), and false negative (FN) as

$$Pr = \frac{TP}{TP+FP} \quad Rc = \frac{TP}{TP+FN} \quad Sp = \frac{TN}{TN+FP}$$
$$Ac = \frac{TP+TN}{TP+FP+TN+FN} \quad DC = \frac{2TP}{2TP+FP+FN}$$
$$G = \sqrt{Rc \times Sp},$$

In our experiments, we use two scales: one at the original image resolution and the other with a subsampling factor of 2. The window size used to compute local average intensity is set to $N = 35$ for original image and is reduced by 5 for the subsampled image. We use $M = 9$ linear structuring elements to apply modified top-hat operation. The lengths of structuring elements L are 30 for original image and 15 for subsampled one.

4.2. Quantitative And Qualitative Comparison

We compare the proposed method with another method proposed in [4], which is specialized in vessel detection in wide-field FA images[3].

Table 1 reports the quantitative comparison in terms of 6 aforementioned metrics for each individual test image and as an average over all pixels across images. Our method significantly outperforms the previous method in [4]. It achieves an average precision of 0.7021, an average recall of 0.6217, and an average specification of 0.9892. Apart from precision, recall, and specification, the results of dice coefficient and G-mean of our methods are normally higher than those in [4] except only on image "GER1". Detailed examination of image "GER1" indicates that this image is captured at early phase after dye injection. As a consequence, only a small portions of vasculature can be seen in this image. We achieve an average accuracy of 0.9787, which is only 0.012 lower than the method in [4].

[3]While a large number of methods have been developed for vessel detection in color fundus images, these methods do not offer competitive performance for the completely different FA modality and are therefore not included in our comparison.

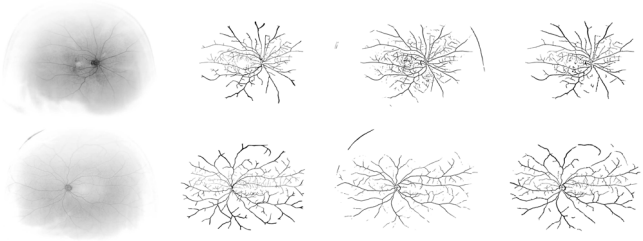

Fig. 5. Sample results of visual comparison of vessel detection using the proposed method and [4]. Columns from left to right: input FA image, ground truth, results obtained by [4] and the propsoed method, respectively.

We also note that the accuracy metric is not particularly meaningful in this problem setting because of the highly imbalanced nature of the datasets (most pixels are non-vessels) and because there is also inherent uncertainty in defining the width.

Figure 5 shows the visual comparison of vessel detection using the proposed method and [4] on VAMPIRE dataset. The top raw is the image "AMD2" and the bottom shows the image "GER4". It can been see that the vessel image from [4] includes false positive that corresponds to retina boundary. Notice that the proposed method performs well even though these are significant different in illumination in the images in Fig. 5.

5. CONCLUSION

In this paper, we proposed a novel method to detect vessels in wide-field FA image. Our approach is motivated by the multiple scales and orientations inherently seen in blood vessels. Using a bank of oriented modified top-hat morphological filters with multi-scale processing, our proposed approach provides accurate detection of blood vessels. Experimental results on VAMPIRE datasets demonstrate that the method significantly outperforms the previous algorithm in terms of precision, recall, specification, dice coefficient, and G-mean metrics.

6. ACKNOWLEDGMENT

We thank the Center for Integrated Research Computing, University of Rochester, for providing access to computational resources.

7. REFERENCES

[1] T. Y. Wong and R. McIntosh, "Systemic associations of retinal microvascular signs: a review of recent population-based studies," *Ophthalmic and Physiological Optics*, vol. 25, no. 3, pp. 195–204, 2005.

[2] S. Rogers, R. L. McIntosh, N. Cheung, L. Lim, J. J. Wang, P. Mitchell, J. W. Kowalski, H. Nguyen, and T. Y. Wong, "The prevalence of retinal vein occlusion: pooled data from population studies from the united states, europe, asia, and australia," *Ophthalmology*, vol. 117, no. 2, pp. 313–319, 2010.

[3] A. Manivannan, J. Plskova, A. Farrow, S. Mckay, P. F. Sharp, and J. V. Forrester, "Ultra-wide-field fluorescein angiography of the ocular fundus," *Amer. J. Ophthalmology*, vol. 140, no. 3, pp. 525–527, 2005.

[4] A. Perez-Rovira, K. Zutis, J. Hubschman, and E. Trucco, "Improving vessel segmentation in ultra-wide field-of-view retinal fluorescein angiograms," in *IEEE Intl. Conf. Eng. in Med. and Biol. Soc.*, 2011, pp. 2614–2617.

[5] C. L. Srinidhi, P. Aparna, and J. Rajan, "Recent advancements in retinal vessel segmentation," *J. Med. Syst.*, vol. 41, no. 4, p. 70, 2017.

[6] M. Niemeijer, J. Staal, B. Van Ginneken, M. Loog, M. D. Abramoff *et al.*, "Comparative study of retinal vessel segmentation methods on a new publicly available database," in *SPIE Medical Imaging*, vol. 5370, 2004, pp. 648–656.

[7] J. I. Orlando, E. Prokofyeva, and M. B. Blaschko, "A discriminatively trained fully connected conditional random field model for blood vessel segmentation in fundus images," *IEEE Trans. Biomed. Eng.*, vol. 64, no. 1, pp. 16–27, 2017.

[8] P. Liskowski and K. Krawiec, "Segmenting retinal blood vessels with deep neural networks," *IEEE Trans. Med. Imaging*, vol. 35, no. 11, pp. 2369–2380, Nov 2016.

[9] D. Maji, A. Santara, P. Mitra, and D. Sheet, "Ensemble of deep convolutional neural networks for learning to detect retinal vessels in fundus images," *arXiv:1603.04833*, 2016.

[10] K.-K. Maninis, J. Pont-Tuset, P. Arbeláez, and L. Van Gool, "Deep retinal image understanding," in *Intl. Conf. Med. Image Computing and Computer-Assisted Intervention*, 2016, pp. 140–148.

[11] J. Son, S. J. Park, and K.-H. Jung, "Retinal vessel segmentation in fundoscopic images with generative adversarial networks," *arXiv:1706.09318*, 2017.

[12] K. Simonyan and A. Zisserman, "Very deep convolutional networks for large-scale image recognition," in *Intl. Conf. Learning Representations*, 2017.

[13] I. Goodfellow, J. Pouget-Abadie, M. Mirza, B. Xu, D. Warde-Farley, S. Ozair, A. Courville, and Y. Bengio, "Generative adversarial nets," in *Adv. in Neural Info. Proc. Sys.*, 2014, pp. 2672–2680.

[14] S. Chaudhuri, S. Chatterjee, N. Katz, M. Nelson, and M. Goldbaum, "Detection of blood vessels in retinal images using two-dimensional matched filters," *IEEE Trans. Med. Imaging*, vol. 8, no. 3, pp. 263–269, Sep 1989.

[15] A. Hoover, V. Kouznetsova, and M. Goldbaum, "Locating blood vessels in retinal images by piecewise threshold probing of a matched filter response," *IEEE Trans. Med. Imaging*, vol. 19, no. 3, pp. 203–210, 2000.

[16] S. S. Kar and S. P. Maity, "Blood vessel extraction and optic disc removal using curvelet transform and kernel fuzzy c-means," *Computers in Biol. and Med.*, vol. 70, pp. 174–189, 2016.

[17] M. Krause, R. M. Alles, B. Burgeth, and J. Weickert, "Fast retinal vessel analysis," *Journal of Real-Time Image Processing*, vol. 11, no. 2, pp. 413–422, 2016.

[18] T. A. Soomro, J. Gao, M. Paul, and L. Zheng, "Retinal blood vessel extraction method based on basic filtering schemes," *IEEE Intl. Conf. Image Proc.*, 2017.

[19] F. Zana and J. C. Klein, "Segmentation of vessel-like patterns using mathematical morphology and curvature evaluation," *IEEE Trans. Image Proc.*, vol. 10, no. 7, pp. 1010–1019, Jul 2001.

[20] E. M. Sigursson, S. Valero, J. A. Benediktsson, J. Chanussot, H. Talbot, and E. Stefánsson, "Automatic retinal vessel extraction based on directional mathematical morphology and fuzzy classification," *Patt. Recogn. Ltrs.*, vol. 47, pp. 164–171, 2014.

[21] P. Burt and E. Adelson, "The laplacian pyramid as a compact image code," *IEEE Trans. Comm.*, vol. 31, no. 4, pp. 532–540, 1983.

[22] J. G. A. e Sousa, C. M. Oliveira, and L. A. da Silva Cruz, "Automatic detection of laser marks in retinal digital fundus images," in *European Signal Proc. Conf.*, 2016, pp. 1313–1317.

[23] R. C. Gonzales and P. Wintz, *Digital Image Processing (2nd Ed.)*. Boston, MA, USA: Addison-Wesley Longman Publishing Co., Inc., 1987.

[24] A. M. Mendonca and A. Campilho, "Segmentation of retinal blood vessels by combining the detection of centerlines and morphological reconstruction," *IEEE Trans. Med. Imaging*, vol. 25, no. 9, pp. 1200–1213, Sept 2006.

[25] N. Otsu, "A threshold selection method from gray-level histograms," *IEEE Intl. Conf. Systems, Man and Cyber.*, vol. 9, no. 1, pp. 62–66, 1979.